

# Identification of Overlapping Communities via Constrained Egonet Tensor Decomposition

Fatemeh Sheikholeslami and Georgios B. Giannakis

Dept. of ECE and Digital Tech. Center, University of Minnesota

Minneapolis, MN 55455, USA

E-mails: {sheik081,georgios}@umn.edu

**Abstract**—Detection of overlapping communities in real-world networks is a generally challenging task. Upon recognizing that a network is in fact the union of its egonets, a novel network representation using multi-way data structures is advocated in this contribution. The introduced sparse tensor-based representation exhibits richer structure compared to its matrix counterpart, and thus enables a more robust approach to community detection. To leverage this structure, a constrained tensor approximation framework is introduced using PARAFAC decomposition. The arising constrained trilinear optimization is handled via alternating minimization, where intermediate subproblems are solved using the alternating direction method of multipliers (ADMM) to ensure convergence. The factors obtained provide soft community memberships, which can further be exploited for crisp, and possibly-overlapping community assignments. The framework is further broadened to include time-varying graphs, where the edgeseet as well as the underlying communities evolve through time. Performance of the proposed approach is assessed via tests on benchmark synthetic graphs as well as real-world networks. As corroborated by numerical tests, the proposed tensor-based representation captures multi-hop nodal connections, that is, connectivity patterns within single-hop neighbors, whose exploitation yields a more robust community identification in the presence of mixing as well as overlapping communities.

**Index Terms**—Community detection, overlapping communities, egonet subgraphs, tensor decomposition, constrained PARAFAC, sparse tensors.

## I. INTRODUCTION

Graph representation of complex real-world networks provides an invaluable tool for analysis and discovery of intrinsic attributes present in social, biological, and financial networks. One such attribute is the presence of small subgraphs, referred to as “communities” or “clusters,” whose dense intra-connections and sparse inter-connections often represents a potential “association” among the participating entities (nodes). The task of community identification targets the discovery of such highly-interwoven nodes, and is of paramount interest in areas as diverse as unveiling functional modules in biological networks such as brain [1], trend analysis in social media [2], [3], and clustering of costumers in recommender systems [4].

Past works on community detection include those based on modularity-maximization [5], [6], generative and statistical models [7]–[9], local-metric optimization [10], spectral clustering [11], and matrix factorization [12]–[16]; see e.g. [17], [18] for a comprehensive overview. With recent

exploratory studies over contemporary real-world networks, new challenges have been raised in community identification, addressing the presence of overlapping communities [19]–[21], multimodal interaction of nodes over multiview networks [22], [23], exploitation of nodal and edge-related side-information [24], as well as dynamic interactions within a network [25], [26].

In handling such new challenges, reliance on the adjacency matrix representation of networks limits their capabilities in capturing higher-order interactions, which can potentially provide critical information via temporal, multi-modal, or even multi-hop connectivity among nodes. To this end, *tensors* as multi-way data structures provide a viable alternative, whose increased representational capabilities can potentially lead to a more informative community identification [22], [23], [25], [27], [28]. For instance, [29] and [30] construct higher-order tensors whose entries are non-zero if a tuple of nodes jointly belongs to a cycle or a clique, while [25] captures temporal dynamics of communities via tensors. Under certain conditions, tensor decompositions are unique [31]–[33], and can guarantee identifiability of the community structure.

The present work develops a novel tensor-based network representation by recognizing that a network is the union of its *egonets*. An egonet is defined per node as the subgraph induced by the node itself, its one-hop neighbors, and all their connections, whose structure has been exploited in anomaly detection [34], and user-specific community identification [35], [36]. By concatenating egonet adjacency matrices along the 3-rd dimension of a three-way tensor, the proposed network representation, named *egonet-tensor*, captures information per node beyond its one-hop connectivity patterns. In fact, in a number of practical networks only adjacency matrix of the network is given, rendering egonets a unique candidate for enhancing community identification performance when extra nodal features are kept private, e.g., Amazon costumers graphs. By construction, egonet-tensor exhibits richer structure compared to its matrix counterpart, which is further exploited by casting the community detection task in a constrained tensor decomposition framework. Building on preliminary results in [28], solvers with convergence guarantees are developed for the proposed constrained non-convex optimization, whose solution yields the community-revealing components, utilized for soft as well as crisp community assignments unveiling possibly *overlapping* communities. The performance of the proposed EgoTen toolbox is compared with its matrix

counterpart as well as state-of-the-art methods, corroborating the improved quality of detected communities through the exploitation of higher-order statistics captured in the egonet-tensor representations. Furthermore, the proposed tensor-based framework is extended for application on time-varying graphs, where network connectivity evolves through time, leading to emergence or disappearance of communities.

The rest of the paper is organized as follows. Section II introduces the novel tensor-based network representation, and Section III presents the constrained tensor decomposition, and its efficient solver for the task of community identification. Performance metrics for evaluating the quality of detected communities in networks with and without ground-truth communities is the subject of Section IV, and Section IV introduces identification of time-varying graphs using the proposed algorithms. Section VI provides numerical tests, while Section VII concludes the paper.

*Notation.* Lower- (upper-) case boldface letters denote column vectors (matrices), and underlined upper-case boldface letters stand for tensor structures. Calligraphic symbols are reserved for sets, while  $T$  stands for transposition. Symbols  $\circ$ ,  $\otimes$  and  $\odot$  are reserved for outer-product, Kronecker-product and Khatri-Rao-product, respectively, and  $\text{Tr}\{\mathbf{X}\}$  denotes the trace of matrix  $\mathbf{X}$ .

## II. EGONET-TENSOR CONSTRUCTION

Consider a graph  $\mathcal{G} = (\mathcal{V}, \mathcal{E}, \mathbf{W})$ , where  $\mathcal{V}$ ,  $\mathcal{E}$ , and  $\mathbf{W} \in \mathbb{R}^{N \times N}$  respectively denote the set of  $N$  nodes, i.e.,  $|\mathcal{V}| = N$ , edges, and the adjacency matrix. In the case of binary networks,  $w_{ij} := 1$  if  $(i, j) \in \mathcal{E}$ , and  $w_{ij} := 0$  otherwise. Furthermore, the *egonet* of node  $n$  is defined as the subgraph induced by node  $n$ , its single-hop neighbors, and all their connections. Let  $\mathcal{G}^{(n)} := (\mathcal{V}, \mathcal{E}^{(n)}, \mathbf{W}^{(n)}) \subset \mathcal{G}$  be the subgraph with  $\mathcal{E}^{(n)}$  the egonet edgeset, and  $\mathbf{W}^{(n)} \in \mathbb{R}^{N \times N}$  the corresponding adjacency matrix whose non-zero support captures the edges in  $\mathcal{E}^{(n)}$ ; that is,

$$w_{ij}^{(n)} := \begin{cases} w_{ij} & \text{if } (i, j) \in \mathcal{E}^{(n)} \\ 0 & \text{otherwise.} \end{cases}$$

Figure 1 (a) illustrates such subgraphs, where the black node corresponds to the central node of the egonet, and the single-hop neighbors are colored green. Typically, the center node  $n$  is excluded from  $\mathcal{G}^{(n)}$ , but it is included here for convenience.

As Figure 1 (b) depicts, graph  $\mathcal{G}$  can now be fully described by a three-way *egonet-tensor*  $\underline{\mathbf{W}} \in \mathbb{R}^{N \times N \times N}$ , where frontal slabs correspond to egonet adjacency matrices  $\{\mathbf{W}^{(n)}\}_{n=1}^N$ , stacked one after the other. In tensor parlance, that is tantamount to setting the  $n$ -th frontal slab as  $\underline{\mathbf{W}}_{:, :, n} := \mathbf{W}^{(n)}$ , where  $:$  is a free index that spans its range.

The advantage of presenting a graph with its egonet-tensor lies in the fact that tensors as higher-order structures are capable of capturing “useful information” along their different dimensions, a.k.a., “modes.” In a network with underlying community structure, the proposed egonet-tensor representation is indeed capable of preserving the inherent “similarities” among egonet adjacencies along the 3-rd mode, whose extraction is crucial in tasks such as community detection.

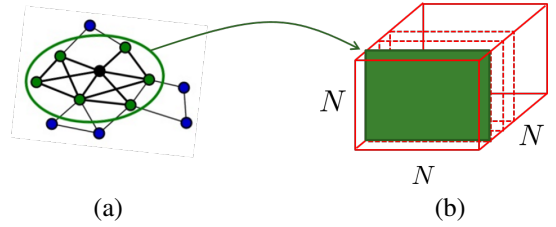


Fig. 1: Construction of *egonet-tensor* with frontal slabs as egonet adjacencies.

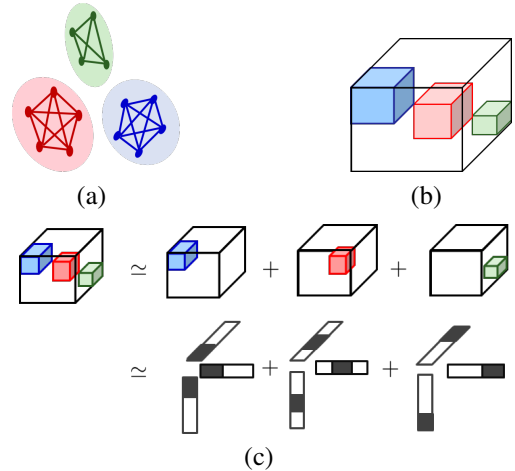


Fig. 2: (a) A toy network with 3 fully connected non-overlapping communities; (b) corresponding egonet-tensor; and (c) its community-revealing factorization via CPD.

Such representation is of particular interest for various settings where no nodal features are provided (that is, only the adjacency matrix is given), making egonets very appealing for an improved network representation as well as the development of robust schemes for the task of interest. The following toy example clarifies how such similarities induce a structure over the egonet tensor, and intuitively discusses how its exploitation can lead to an improved performance.

### A. Toy example

Let us consider a toy network with three fully-connected communities, illustrated in Figure 3 (a). Since each node is a member of a *fully-connected* community, the binary adjacency matrix of its egonet is identical to that of any other node in its resident community. Furthermore, after permutation, this egonet adjacency matrix consists of a single block of nonzero entries (with zero diagonal entries if the network is free of self-loops), and zeros elsewhere. This implies that the egonet-tensor can be permuted similarly into a block-diagonal tensor with three nonzero blocks, as illustrated in Figure 3 (b).

Adopting the well-known canonical polyadic decomposition (CPD) to decompose  $\underline{\mathbf{W}}$  into its constituent rank-one tensors, the model naturally approximates the tensor with rank three, thus revealing the number of underlying communities. In fact, if the diagonal entries were all set to 1, i.e. considering

self loops for all the neighboring nodes in an egonet, this approximation would be exact; see Figure 3 (c).

In practice, real-world networks often demonstrate overlapping community structure, where some nodes are associated with multiple communities rather than a single one. To address such cases, consider the augmented network in Figure 3 (a), where a new node (or a super node corresponding to more than one node) associated with two communities is added. Once the corresponding egonet tensor is constructed, the presence of overlapping communities manifests itself in overlapping diagonal blocks in the egonet tensor; see Figure 3 (b) in comparison with disjoint blocks in Figure 2 (b). As it will become evident in Section II, by exploiting a structured CPD on the arising egonet-tensor, it can be shown that the frontal slab corresponding to the egonet adjacency of an overlapping node is approximated by multiple summands, each corresponding to one of its resident communities. Figure 3 (c) illustrates how the obtained decomposition reveals the multi-community association of the augmented node based on its egonet adjacency matrix. The egonet-tensor representation naturally trades off flexibility for increased redundancy and memory costs. Nevertheless, the resulting tensor is extremely sparse, and off-the-shelf tools for sparse tensor computations can be readily utilized; see e.g., [37]–[39].

Unfortunately, such idealistic assumptions where each community is fully-connected within and well-separated from other communities, are not fulfilled in real-world networks. Nevertheless, the inherent similarities among egonet adjacencies induce a potentially useful reinforced structure along the 3<sup>rd</sup> mode of the proposed egonet-tensor representation. For instance, nodes in a community often exhibit dense (rather than full) connections among themselves, and fewer connections with other communities. This property is consequently reflected in the egonet-tensor (as well as the traditional matrix adjacency) representation by dense diagonal blocks, whose clear separation fades away as *out-of-community connections* increase. However, the presence of overlapping communities can further smear the block-structure as overlapping nodes are “well-connected” with multiple communities. The performance of traditional community detection methods often dramatically degrades in networks with such properties, whereas exploiting the *structured redundancy* offered via the proposed egonet-tensor representation and casting the problem in a community-revealing tensor decomposition framework increases robustness against the aforementioned phenomena.

### III. CONSTRAINED TENSOR DECOMPOSITION

Given  $\underline{\mathbf{W}}$ , this section leverages the canonical polyadic decomposition (CPD) [37] in order to factorize the egonet tensor into its constituent community-revealing factors. Assuming that the number of communities is upperbounded by  $K$ , a rank- $K$  CPD model is sought by solving the following constrained least-squares (LS) problem

$$\begin{aligned} \{\hat{\mathbf{A}}, \hat{\mathbf{B}}, \hat{\mathbf{C}}\} = \arg \min_{\mathbf{A}, \mathbf{B}, \mathbf{C}} \quad & \|\underline{\mathbf{W}} - \sum_{k=1}^K \mathbf{a}_k \circ \mathbf{b}_k \circ \mathbf{c}_k\|_F^2 \\ \text{s.t.} \quad & \mathbf{A} \geq \mathbf{0}, \mathbf{B} \geq \mathbf{0}, \mathbf{C} \geq \mathbf{0} \end{aligned} \quad (1)$$

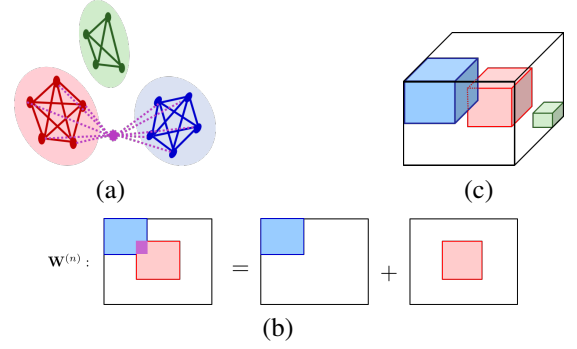


Fig. 3: (a) A toy network with overlapping communities; (b) corresponding egonet-tensor; and (c) community-revealing approximation of egonet adjacency of the shared node via CPD.

where  $\mathbf{A} := [\mathbf{a}_1, \dots, \mathbf{a}_K] \in \mathbb{R}^{N \times K}$ ,  $\mathbf{B} := [\mathbf{b}_1, \dots, \mathbf{b}_K] \in \mathbb{R}^{N \times K}$ , and  $\mathbf{C} := [\mathbf{c}_1, \dots, \mathbf{c}_K] \in \mathbb{R}^{N \times K}$ ; while the term  $(\mathbf{a}_k \circ \mathbf{b}_k \circ \mathbf{c}_k)$  is the outer product of the three vectors, which induces the  $k$ -th rank-one tensor component in the rank- $K$  decomposition; see [37] for further details on CPD. The constraint  $\mathbf{A} \geq \mathbf{0}$  denotes entry-wise nonnegativity constraints, i.e.,  $a_{nk} \geq 0$  for  $n = 1, \dots, N$  and  $k = 1, \dots, K$ ; and similarly for factors  $\mathbf{B}$  and  $\mathbf{C}$ . These constraints enforce the nonnegativity of egonet adjacency matrices, thus inducing structure in the sought CPD and providing interpretation of the decomposition factors.

It is possible to re-write (1) as, see e.g., [37]

$$\begin{aligned} \{\hat{\mathbf{A}}, \hat{\mathbf{B}}, \hat{\mathbf{C}}\} = \arg \min_{\mathbf{A}, \mathbf{B}, \mathbf{C}} \quad & \sum_{n=1}^N \|\mathbf{W}^{(n)} - \mathbf{A} \text{diag}(\tilde{\mathbf{c}}_n) \mathbf{B}^\top\|_F^2 \\ \text{s.t.} \quad & \mathbf{A} \geq \mathbf{0}, \mathbf{B} \geq \mathbf{0}, \mathbf{C} \geq \mathbf{0} \end{aligned}$$

where  $\text{diag}(\tilde{\mathbf{c}}_n)$  is a diagonal matrix holding the  $n$ -th row of  $\mathbf{C}$  on its diagonal. Focusing on the  $n$ -th frontal slab of the egonet-tensor, CPD provides the approximation

$$\mathbf{W}^{(n)} = \sum_{k=1}^K c_{nk} (\mathbf{a}_k \mathbf{b}_k^\top) \quad (2)$$

where  $c_{nk}$  denotes the  $(n, k)$ -th entry of factor  $\mathbf{C}$ . Such decomposition can be interpreted as a weighted sum over  $K$  “basis”,  $\{\mathbf{a}_k \mathbf{b}_k^\top\}_{k=1}^K$ , where  $(\mathbf{a}_k \mathbf{b}_k^\top)$  captures the “connectivity structure” within the  $k$ -th community. Consequently,  $c_{nk}$  can be viewed as *association level* of node  $n$  to community  $k$  for  $k = 1, \dots, K$ . Furthermore, one can easily realize that since  $(\mathbf{a}_k \mathbf{b}_k^\top)$  is viewed as connectivity structure of community  $k$ , the elements in  $\mathbf{a}_k := [a_{1k}, \dots, a_{nk}]^\top$  and  $\mathbf{b}_k := [b_{1k}, \dots, b_{nk}]^\top$  can be consequently viewed as the *contribution levels* of nodes  $n = 1, \dots, N$  to community  $k$ . This interpretation of the factors, prompts us to further leverage the structure and introduce additional constraints on the CPD factors.

#### A. Structured CPD

Real-world networks often involve nodes which are associated with more than one community, resulting in multiple

nonzero entries in the association vector  $[c_{n1}, c_{n2}, \dots, c_{nK}]$  corresponding to a generic node  $n$ . To return a normalized association vector, we augment the optimization in (1) by the constraints  $\sum_{k=1}^K c_{nk} = 1$  for  $n = 1, 2, \dots, N$ , which together with  $\mathbf{C} \geq \mathbf{0}$  acts as a simplex constraint on the rows of  $\mathbf{C}$ . Upon imposing simplex constraints the CPD is further regularized as

$$\begin{aligned} \{\widehat{\mathbf{A}}, \widehat{\mathbf{B}}, \widehat{\mathbf{C}}\} = & \arg \min_{\mathbf{A}, \mathbf{B}, \mathbf{C}} \left\{ \|\underline{\mathbf{W}} - \sum_{k=1}^K \mathbf{a}_k \circ \mathbf{b}_k \circ \mathbf{c}_k\|_F^2 \right. \\ & \left. + \lambda (\|\mathbf{A}\|_F^2 + \|\mathbf{B}\|_F^2) \right\} \\ \text{s.t. } & \mathbf{A} \geq \mathbf{0}, \mathbf{B} \geq \mathbf{0}, \mathbf{C} \geq \mathbf{0} \\ & \|\tilde{\mathbf{c}}_n\|_1 = 1 \quad \forall n = 1, 2, \dots, N \end{aligned} \quad (3)$$

Different from [40] and [41], the regularization term  $\|\mathbf{A}\|_F^2 + \|\mathbf{B}\|_F^2$  does not play the role of rank-regularization for subspace learning, instead it solves the scalar ambiguity in factors  $\mathbf{A}$  and  $\mathbf{B}$ .

The CPD problem formulated in (3) is a tri-linear constrained LS problem, whose minimization can be tackled by alternating optimization. In the ensuing subsection, the proposed solver is developed using by alternating optimization with ADMM intermediate steps; see e.g. [42] and [43].

### B. Solving the proposed structured CPD

In the proposed alternating optimization scheme, each step consists of fixing two factors and minimizing the arising subproblem with respect to the third factor. In this subsection, we study the emerging sub-problems and propose efficient solvers for tackling those.

1) *Factor A update:* Consider first the update of factor  $\mathbf{A}$  at iteration  $k$ , obtained after fixing  $\mathbf{B} = \mathbf{B}^{(k-1)}$  and  $\mathbf{C} = \mathbf{C}^{(k-1)}$  and solving the corresponding minimization. The arising subproblem, after algebraic manipulation can be re-written as

$$\mathbf{A}^{(k)} = \arg \min_{\mathbf{A} \geq \mathbf{0}} \|\mathbf{W}_1 - (\mathbf{B}^{(k-1)} \odot \mathbf{C}^{(k-1)}) \mathbf{A}^\top\|_F^2 + \lambda \|\mathbf{A}\|_F^2 \quad (4)$$

where  $\mathbf{W}_1 := [\text{vec}(\underline{\mathbf{W}}_{1,:}), \dots, \text{vec}(\underline{\mathbf{W}}_{N,:})] \in \mathbf{R}^{N^2 \times N}$  is a matricized reshaping of the tensor  $\underline{\mathbf{W}}$ . Also  $\mathbf{B}^{(k-1)} \odot \mathbf{C}^{(k-1)} := [\mathbf{b}_1^{(k-1)} \otimes \mathbf{c}_1^{(k-1)}, \dots, \mathbf{b}_K^{(k-1)} \otimes \mathbf{c}_K^{(k-1)}]$  is the Khatri-Rao product of  $\mathbf{B}^{(k-1)}$  and  $\mathbf{C}^{(k-1)}$ , where  $\mathbf{b}_i^{(k-1)}$  ( $\mathbf{c}_i^{(k-1)}$ ) denotes column  $i$  of  $\mathbf{B}^{(k-1)}$  (resp.  $\mathbf{C}^{(k-1)}$ ), and  $\otimes$  denotes the Kronecker product operator; see also [37].

Following the steps in [43], auxiliary variable  $\bar{\mathbf{A}}$  is introduced to account for the nonnegativity constraint, and the augmented Lagrangian of (4) is

$$\begin{aligned} \mathcal{L}_A^{(k)}(\mathbf{A}, \bar{\mathbf{A}}, Y) = & \|\mathbf{W}_1 - \mathbf{H}_A^{(k)} \mathbf{A}^\top\|_F^2 + \lambda \text{Tr}\{\mathbf{A} \mathbf{A}^\top\} \\ & + r_+(\bar{\mathbf{A}}) + (\rho/2) \|\mathbf{Y} + \mathbf{A} - \bar{\mathbf{A}}\|_F^2 \end{aligned} \quad (5)$$

where  $\bar{\mathbf{A}}, \mathbf{Y} \in \mathbf{R}^{N \times K}$ ,  $\mathbf{H}_A^{(k)} := \mathbf{C}^{(k-1)} \odot \mathbf{B}^{(k-1)}$ , and  $r_+(\bar{\mathbf{A}})$  is the regularizer corresponding to the nonnegativity constraint,

$$r_+(\bar{\mathbf{A}}) := \begin{cases} 0 & \text{if } \bar{\mathbf{A}} \geq \mathbf{0} \\ +\infty & \text{o.w.} \end{cases}$$

The ADMM solver then proceeds by iteratively updating blocks of variables  $\mathbf{A}, \bar{\mathbf{A}}, \mathbf{Y}$  as

$$\begin{cases} \mathbf{A}^{(r)} = \arg \min_{\mathbf{A}} \mathcal{L}_A^{(k)}(\mathbf{A}, \bar{\mathbf{A}}^{(r-1)}, \mathbf{Y}^{(r-1)}) \\ \bar{\mathbf{A}}^{(r)} = \mathcal{P}_+(\mathbf{Y}^{(r-1)} + \mathbf{A}^{(r)}) \\ \mathbf{Y}^{(r)} = \mathbf{Y}^{(r-1)} - \rho(\mathbf{A}^{(r)} - \bar{\mathbf{A}}^{(r)}) \\ r = r + 1 \end{cases} \quad (6)$$

until a convergence criterion is met, namely whether the maximum number of iterations is exceeded, i.e.,  $r = I_{\max, \text{ADMM}}$ , or a prescribed  $\epsilon$ -accuracy is met, i.e.,  $\|\mathbf{A}^{(r)} - \mathbf{A}^{(r-1)}\|_F / \|\mathbf{A}^{(r-1)}\|_F < \epsilon$ . Operator  $\mathcal{P}_+(\cdot)$  in (6) denotes the element-wise projection of the input matrix onto the positive orthant, and its use enables the  $\bar{\mathbf{A}}^{(r)}$  update to be carried at a very low cost. The Lagrange multiplier is set to  $\rho = \|\mathbf{H}_A\|_F^2 / K$  - a value that is empirically shown to yield similar performance to that of the optimal value [43]. The final  $\bar{\mathbf{A}}^{(r)}$  iterate in the ADMM solver will be used to update  $\mathbf{A}^{(k)}$ .

2) *Factor B update:* Update of factor  $\mathbf{B}$  can be similarly carried out by solving the subproblem

$$\mathbf{B}^{(k)} = \arg \min_{\mathbf{B} \geq \mathbf{0}} \|\mathbf{W}_2 - \mathbf{H}_B^{(k)} \mathbf{B}^\top\|_F^2 + \lambda \|\mathbf{B}\|_F^2 \quad (7)$$

where  $\mathbf{W}_2 := [\text{vec}(\underline{\mathbf{W}}_{:,1}), \dots, \text{vec}(\underline{\mathbf{W}}_{:,N})]$ , and  $\mathbf{H}_B^{(k)} := \mathbf{C}^{(k-1)} \odot \mathbf{A}^{(k)}$ , yielding a similar optimization problem as in (4). Algorithm 2 tabulates the explicit update rules for solving (4) and similarly (7) using a general framework.

3) *Factor C update:* Update of factor  $\mathbf{C}$  is obtained by fixing  $\mathbf{A}$  and  $\mathbf{B}$  at their most recent values, and solving the subproblem

$$\begin{aligned} \mathbf{C}^{(k)} = & \arg \min_{\mathbf{C}} \|\mathbf{W}_3 - (\mathbf{A}^{(k)} \odot \mathbf{B}^{(k)}) \mathbf{C}^\top\|_F^2 \\ \text{s.t. } & \mathbf{C} \geq \mathbf{0} \quad \|\tilde{\mathbf{c}}_n\|_1 = 1 \quad \forall n = 1, \dots, N \end{aligned} \quad (8)$$

where  $\mathbf{W}_3 := [\text{vec}(\underline{\mathbf{W}}_{:,1}), \dots, \text{vec}(\underline{\mathbf{W}}_{:,N})]$ . Utilizing an ADMM approach, the augmented Lagrangian is formed as

$$\begin{aligned} \mathcal{L}_C^{(k)}(\mathbf{C}, \bar{\mathbf{C}}, Y) = & \|\mathbf{W}_3 - \mathbf{H}_C^{(k)} \mathbf{C}^\top\|_F^2 + r_{\text{simp}}(\bar{\mathbf{C}}) \\ & + (\rho/2) \|\mathbf{Y} + \mathbf{C} - \bar{\mathbf{C}}\|_F^2 \end{aligned} \quad (9)$$

where  $\bar{\mathbf{C}}, \mathbf{Y} \in \mathbf{R}^{N \times K}$ ,  $\mathbf{H}_C^{(k)} := (\mathbf{A}^{(k)} \odot \mathbf{B}^{(k)})$ , and  $r_{\text{simp}}(\bar{\mathbf{C}})$  is the regularizer corresponding to the simplex constraint on the rows of matrix  $\bar{\mathbf{C}}$  as

$$r_{\text{simp}}(\bar{\mathbf{C}}) := \begin{cases} 0 & \text{if } \bar{\mathbf{C}} \geq \mathbf{0}, \sum_{k=1}^K \bar{c}_{n,k} = 1 \quad \forall n \\ +\infty & \text{o.w.} \end{cases}$$

ADMM solver then proceeds with iterative updates as

$$\begin{cases} \mathbf{C}^{(r)} = \arg \min_{\mathbf{C}} \mathcal{L}_C^{(k)}(\mathbf{C}, \bar{\mathbf{C}}^{(r-1)}, \mathbf{Y}^{(r-1)}) \\ \bar{\mathbf{C}}^{(r)} = \mathcal{P}_{\text{simp}}(\mathbf{Y}^{(r-1)} + \mathbf{C}^{(r)}) \\ \mathbf{Y}^{(r)} = \mathbf{Y}^{(r-1)} - \rho(\mathbf{C}^{(r)} - \bar{\mathbf{C}}^{(r)}) \\ r = r + 1 \end{cases} \quad (10)$$

where  $\mathcal{P}_{\text{simp}}(\cdot)$  denotes the projection of rows of the input matrix onto the simplex set. This projection has been widely studied and can be efficiently accommodated by the algorithm discussed in [44]. Explicit update steps of the ADMM solver for (8) are tabulated under Algorithm 3.

---

**Algorithm 1** Constrained tensor decomposition via alternating least-squares (ALS)

---

Input  $\underline{\mathbf{W}}, K, I_{\max}, \lambda$   
Initialize  $\mathbf{A}, \mathbf{B}, \mathbf{C} \in \mathbb{R}^{N \times K}$  at random and set  $k = 0$   
Form Matrix reshapes  $\mathbf{W}_1, \mathbf{W}_2, \mathbf{W}_3$  of the tensor as  
 $\mathbf{W}_1 := [\text{vec}(\underline{\mathbf{W}}_{1,:,:}), \dots, \text{vec}(\underline{\mathbf{W}}_{N,:,:})]$   
 $\mathbf{W}_2 := [\text{vec}(\underline{\mathbf{W}}_{:,1,:}), \dots, \text{vec}(\underline{\mathbf{W}}_{:,N,:})]$   
 $\mathbf{W}_3 := [\text{vec}(\underline{\mathbf{W}}_{:,:,1}), \dots, \text{vec}(\underline{\mathbf{W}}_{:,:,N})]$   
**while**  $k < I_{\max}$  **do** or not-converged  
 $\mathbf{H}_A^{(k)} = \mathbf{C}^{(k-1)} \odot \mathbf{B}^{(k-1)}$   
 $\mathbf{A}^{(k)} \leftarrow$  Algorithm 2 with input  $\{\mathbf{H}_A^{(k)}, \mathbf{W}_1, \mathbf{A}^{(k-1)}\}$   
 $\mathbf{H}_B^{(k)} = \mathbf{C}^{(k-1)} \odot \mathbf{A}^{(k)}$   
 $\mathbf{B}^{(k)} \leftarrow$  Algorithm 2 with input  $\{\mathbf{H}_B^{(k)}, \mathbf{W}_2, \mathbf{B}^{(k-1)}\}$   
 $\mathbf{H}_C^{(k)} = \mathbf{B}^{(k)} \odot \mathbf{A}^{(k)}$   
 $\mathbf{C}^{(k)} \leftarrow$  Algorithm 3 with input  $\{\mathbf{H}_C^{(k)}, \mathbf{W}_3, \mathbf{C}^{(k-1)}\}$   
 $k \leftarrow k + 1$   
**end while**  
**Retrun**  $\mathbf{A}^{(k)}, \mathbf{B}^{(k)}, \mathbf{C}^{(k)}$

---

**Algorithm 2** ADMM solver for 1<sup>st</sup> and 2<sup>nd</sup> mode subproblems

---

Input  $\mathbf{H}, \mathbf{W}, \mathbf{Z}_{\text{init}}$   
**Goal is to solve**  
 $\mathbf{Z}^* = \arg \min_{\mathbf{Z} \geq \mathbf{0}} \text{Tr} \left\{ \mathbf{Z}(\mathbf{H}^\top \mathbf{H} + \lambda \mathbf{I}_{K \times K}) \mathbf{Z}^\top - 2\mathbf{W}^\top \mathbf{H} \mathbf{Z}^\top \right\}$   
Set  $\rho = \frac{\|\mathbf{Z}_{\text{init}}\|_F^2}{K}, \mathbf{Z}^{(0)} = \mathbf{Z}_{\text{init}}, \bar{\mathbf{Z}}^{(0)} = \mathbf{0}_{N \times K}, \mathbf{Y}^{(0)} = \mathbf{0}_{N \times K}, r = 0$   
**while**  $r < I_{\max, \text{ADMM}}$  **do**  
 $\mathbf{Z}^{(r)} = (\mathbf{H}^\top \mathbf{H} + (\lambda + \rho/2) \mathbf{I}_{K \times K})^{-1}$   
 $\quad \times \left( \mathbf{W}^\top \mathbf{H} + \frac{\rho}{2} (\mathbf{Y}^{(r-1)} - \bar{\mathbf{Z}}^{(r-1)}) \right)$   
 $\bar{\mathbf{Z}}^{(r)} = \mathcal{P}_+ \left( \mathbf{Z}^{(r)} + \mathbf{Y}^{(r-1)} \right)$   
 $\mathbf{Y}^{(r)} = \mathbf{Y}^{(r-1)} - \rho (\mathbf{Z}^{(r)} - \bar{\mathbf{Z}}^{(r)})$   
 $r = r + 1$   
**end while**  
**Retrun**  $\bar{\mathbf{Z}}^{(r)}$

---

**Proposition** If the sequence generated by Alg. 4 is bounded, then the sequence  $\{\mathbf{A}^{(k)}, \mathbf{B}^{(k)}, \mathbf{C}^{(k)}\}$  converges to a stationary point of (3).

**Proof:** The convergence follows from [43, Theorem 1].

#### IV. COMMUNITY ASSIGNMENT AND EVALUATION

Once the proposed solver returns the solution of (3), the rows of factor  $\hat{\mathbf{C}}$  provide a ‘‘soft’’ or ‘‘fuzzy’’ community membership for the nodes in the network. In the special case of networks with non-overlapping communities, using the  $n$ -th row of matrix  $\hat{\mathbf{C}}$ , node  $n$  will be assigned to the community  $k^*$  where  $k^* = \arg \max_{k=1, \dots, K} \hat{c}_{nk}$ .

In order to provide a ‘‘crisp’’ community association in networks *with* overlapping communities, where a node can be associated with more than one community, the entries  $\hat{c}_{nk}$  are compared with a threshold  $\tau$  and node  $n$  is associated with

---

**Algorithm 3** ADMM solver for 3<sup>rd</sup> mode subproblem

---

**Input**  $\mathbf{H}, \mathbf{W}, \mathbf{Z}_{\text{init}}$

**Goal is to solve**

$$\mathbf{Z}^* = \arg \min_{\mathbf{Z} \geq \mathbf{0} \|\bar{\mathbf{z}}_n\|_1=1 \forall n=1, \dots, N} \text{Tr} \left\{ \mathbf{Z} \mathbf{H}^\top \mathbf{H} \mathbf{Z}^\top - 2\mathbf{W}^\top \mathbf{H} \mathbf{Z}^\top \right\}$$

Set  $\rho = \frac{\|\mathbf{Z}_{\text{init}}\|_F^2}{K}, \mathbf{Z}^{(0)} = \mathbf{Z}_{\text{init}}, \bar{\mathbf{Z}}^{(0)} = \mathbf{0}_{N \times K}, \mathbf{Y}^{(0)} = \mathbf{0}_{N \times K}, r = 0$

**while**  $r < I_{\max, \text{ADMM}}$  **do**

$$\mathbf{Z}^{(r)} = (\mathbf{H}^\top \mathbf{H} + \rho/2 \mathbf{I}_{N \times N})^{-1}$$

$$\quad \times \left( \mathbf{W}^\top \mathbf{H} + \frac{\rho}{2} (\mathbf{Y}^{(r-1)} - \bar{\mathbf{Z}}^{(r-1)}) \right)$$

$$\bar{\mathbf{Z}}^{(r)} = \mathcal{P}_{\text{simp}} \left( \mathbf{Z}^{(r)} + \mathbf{Y}^{(r-1)} \right)$$

$$\mathbf{Y}^{(r)} = \mathbf{Y}^{(r-1)} - \rho (\mathbf{Z}^{(r)} - \bar{\mathbf{Z}}^{(r)})$$

$$r = r + 1$$

**end while**

**Retrun**  $\bar{\mathbf{Z}}^{(r)}$

---

community  $k$  if  $\hat{c}_{nk} > \tau$ . Thus, crisp community membership matrix  $\mathbf{\Gamma} \in \mathbb{R}^{N \times K}$  is obtained as

$$[\mathbf{\Gamma}]_{nk} := \begin{cases} 1 & \text{if } \hat{c}_{nk} > \tau \\ 0 & \text{o.w.} \end{cases} \quad \forall n, k \quad (11)$$

There are a number of metrics available for evaluating the quality of a detected *cover*, that is, a set of communities, in networks with underlying community structure. Depending on whether the ground-truth communities are available or not, two categories of metrics are considered.

##### A. Networks with ground-truth communities

Normalized mutual information and F1-score are the most commonly-used metrics for performance evaluation over networks with ground truth communities. Let cover  $\hat{\mathcal{S}} := \{\hat{\mathcal{C}}_1, \dots, \hat{\mathcal{C}}_{|\hat{\mathcal{S}}|}\}$  denote the set of detected communities, where  $\mathcal{C}_i$  is the set of nodes associated with community  $i$  for  $i = 1, 2, \dots, |\hat{\mathcal{S}}|$ , and let the ground truth communities be denoted by  $\mathcal{S}^* := \{\mathcal{C}_1^*, \dots, \mathcal{C}_{|\mathcal{S}^*|}^*\}$ .

**Normalized mutual information (NMI)** [17]: NMI is an information-theoretic metric defined as (cf. [17])

$$\text{NMI}(\mathcal{S}^*, \hat{\mathcal{S}}) := \frac{2\mathcal{I}(\mathcal{S}^*, \hat{\mathcal{S}})}{\mathcal{H}(\mathcal{S}^*) + \mathcal{H}(\hat{\mathcal{S}})}$$

where  $\mathcal{H}(\hat{\mathcal{S}})$  denotes the entropy of set  $\hat{\mathcal{S}}$  defined as

$$\mathcal{H}(\hat{\mathcal{S}}) := - \sum_{i=1}^{|\hat{\mathcal{S}}|} p(\hat{\mathcal{C}}_i) \log p(\hat{\mathcal{C}}_i) = - \sum_{i=1}^{|\hat{\mathcal{S}}|} \frac{|\hat{\mathcal{C}}_i|}{N} \log \frac{|\hat{\mathcal{C}}_i|}{N}$$

and similarly for  $\mathcal{H}(\mathcal{S}^*)$ . Furthermore,  $\mathcal{I}(\mathcal{S}^*, \hat{\mathcal{S}})$  denotes the mutual information between the detected and ground-truth

communities, and is defined as

$$I(\mathcal{S}^*, \hat{\mathcal{S}}) := \sum_{i=1}^{|\mathcal{S}^*|} \sum_{j=1}^{|\hat{\mathcal{S}}|} p(\mathcal{C}_i^* \cap \hat{\mathcal{C}}_j) \log \frac{p(\mathcal{C}_i^* \cap \hat{\mathcal{C}}_j)}{p(\mathcal{C}_i^*)p(\hat{\mathcal{C}}_j)} \quad (12)$$

$$= \sum_{i=1}^{|\mathcal{S}^*|} \sum_{j=1}^{|\hat{\mathcal{S}}|} \frac{|\mathcal{C}_i^* \cap \hat{\mathcal{C}}_j|}{N} \log \frac{N|\mathcal{C}_i^* \cap \hat{\mathcal{C}}_j|}{|\mathcal{C}_i^*||\hat{\mathcal{C}}_j|} \quad (13)$$

Intuitively, mutual information  $I(\mathcal{S}^*, \hat{\mathcal{S}})$  reflects a measure of similarity between the two community sets, while entropy  $H(\hat{\mathcal{S}})$  ( $H(\mathcal{S}^*)$ ) denotes the level of uncertainty in community affiliation of a random node in cover  $\hat{\mathcal{S}}$  (resp.  $\mathcal{S}^*$ ). Thus, high values of NMI, namely its maximum at 1, reflect *predictability* of  $\hat{\mathcal{S}}$  based on  $\mathcal{S}^*$  which readily translates into correct community identification in the detected cover  $\hat{\mathcal{S}}$ , whereas low values of NMI, namely its minimum at 0, reflects poor discovery of the true underlying communities. This measure has been generalized for overlapping communities in [45], and will be utilized for performance assessment in such networks.

**Average F1-score** [9]: F1-score is a measure of binary classification accuracy, specifically, the harmonic mean of *precision* and *recall*, taking its highest value at 1 and lowest value at 0. To obtain the average F1-score for  $\hat{\mathcal{S}}$ , one needs to find which detected community  $\hat{\mathcal{C}}_i \in \hat{\mathcal{S}}$  corresponds to a given true community  $\mathcal{C}_j^* \in \mathcal{S}^*$ , i.e., maximizes the corresponding F1-score. The average F1-score is then given by

$$\bar{F1} := \frac{1}{|\mathcal{S}^*|} \sum_{i=1}^{|\mathcal{S}^*|} F1(\mathcal{C}_i^*, \hat{\mathcal{C}}_{I(i)})$$

where

$$I(i) = \arg \max_j F1(\mathcal{C}_i^*, \hat{\mathcal{C}}_j)$$

$$\text{in which } F1(\mathcal{C}_i^*, \hat{\mathcal{C}}_j) := \frac{2|\mathcal{C}_i^* \cap \hat{\mathcal{C}}_j|}{|\mathcal{C}_i^*| + |\hat{\mathcal{C}}_j|}.$$

### B. Networks without ground-truth communities

A general metric for evaluating the “quality” of detected communities, regardless of whether the ground-truth memberships are available or not, is to measure *conductance* [46].

**Conductance:** Conductance of a detected community  $\hat{\mathcal{C}}_k$  in graph  $\mathcal{G}$  is defined as

$$\phi(\hat{\mathcal{C}}_k) := \frac{\sum_{i \in \hat{\mathcal{C}}_k, j \notin \hat{\mathcal{C}}_k} \mathbf{W}_{ij}}{\min\{\text{vol}(\hat{\mathcal{C}}_k), \text{vol}(\mathcal{V} \setminus \hat{\mathcal{C}}_k)\}}$$

where

$$\text{vol}(\hat{\mathcal{C}}_k) := \sum_{i \in \hat{\mathcal{C}}_k, j \in \hat{\mathcal{C}}_k} \mathbf{W}_{ij}$$

and  $(\mathcal{V} \setminus \hat{\mathcal{C}}_k)$  is the complement of  $\hat{\mathcal{C}}_k$ . According to this measure, *high-quality* communities yield small conductance scores as they exhibit dense connections among the nodes within the community and sparse connections with the rest.

Furthermore, the weighted-average  $\bar{\phi}(\hat{\mathcal{S}})$  is defined as the average conductance of the detected communities weighted by their (normalized) community size, that is,

$$\bar{\phi}(\hat{\mathcal{S}}) := \sum_{k=1}^{|\hat{\mathcal{S}}|} \frac{|\hat{\mathcal{C}}_k|}{N} \phi(\hat{\mathcal{C}}_k). \quad (14)$$

## V. COMMUNITY DETECTION ON TIME-VARYING GRAPHS

In this section, we extend the introduced overlapping community identification approach over networks for which the connectivity evolves over time. For instance, consider the emergence of a new sports club giving rise to a new community of individuals whose newly-formed interactions in the club will be reflected in their connections over the social media, or, the network of brain regions where the activation/deactivation of different regions during a certain task can be captured by a time-varying graph. The goal is to utilize the proposed EgoTen approach for identification of dynamic communities, as well as the corresponding time-varying association of nodes.

To this end, consider graph  $\mathcal{G}_t := (\mathcal{V}, \mathcal{E}_t, \mathbf{W}_t)$ , where the subscript  $t$  denotes time index  $t = 1, \dots, T$ . The set of nodes  $\mathcal{V}$  is assumed fixed across time, while the edgeset  $\mathcal{E}_t$  as well as the corresponding adjacency matrix  $\mathbf{W}_t$  are allowed to vary. The introduced EgoTen community identification algorithm can be readily applied to time-varying graphs as follows.

For any slot  $t$ , the procedure of egonet tensor construction can be carried out, giving rise to a 3-dimensional egonet-tensor denoted by  $\underline{\mathbf{W}}_t$ . Subsequently, the overall 4-dimensional egonet-tensor is constructed by stacking  $\underline{\mathbf{W}}_t \forall t$  along the fourth dimension of  $\underline{\mathbf{W}} \in \mathbb{R}^{N \times N \times N \times T}$ ; that is, according to the tensor parlance we have  $\underline{\mathbf{W}}_{:, :, :, t} = \underline{\mathbf{W}}_t$  for  $t = 1, \dots, T$ . Having formed the overall egonet-tensor  $\underline{\mathbf{W}}$ , dynamic community detection is now cast as

$$\begin{aligned} \{\hat{\mathbf{A}}, \hat{\mathbf{B}}, \hat{\mathbf{C}}, \hat{\mathbf{D}}\} = \arg \min_{\mathbf{A}, \mathbf{B}, \mathbf{C}, \mathbf{D}} & \left\{ \|\underline{\mathbf{W}} - \sum_{k=1}^K \mathbf{a}_k \circ \mathbf{b}_k \circ \mathbf{c}_k \circ \mathbf{d}_k\|_F^2 \right. \\ & \left. + \lambda(\|\mathbf{A}\|_F^2 + \|\mathbf{B}\|_F^2) \right\} \quad (15) \\ \text{s.t.} & \quad \mathbf{A} \geq \mathbf{0}, \mathbf{B} \geq \mathbf{0}, \mathbf{C} \geq \mathbf{0}, \mathbf{D} \geq \mathbf{0} \\ & \quad \|\tilde{\mathbf{c}}_n\|_1 = 1 \quad \forall n = 1, 2, \dots, N \\ & \quad \|\tilde{\mathbf{d}}_n\|_1 = 1 \quad \forall n = 1, 2, \dots, N \end{aligned}$$

where  $\mathbf{A}, \mathbf{B}, \mathbf{C} \in \mathbb{R}^{N \times K}$ , and  $\mathbf{D} := [\tilde{\mathbf{d}}_1^\top, \dots, \tilde{\mathbf{d}}_T^\top]^\top \in \mathbb{R}^{T \times K}$ . The LS cost in (15) is the generalization of that for the 3-dimensional tensor decomposition to a higher dimension, while nonnegativity and simplex constrains are similarly carried over for  $\mathbf{D}$ . To clarify the simplex constraints on the rows of  $\mathbf{D}$ , consider the decomposition

$$\underline{\mathbf{W}}_t = \sum_{k=1}^K d_{tk} (\mathbf{a}_k \circ \mathbf{b}_k \circ \mathbf{c}_k). \quad (16)$$

For a fixed slot  $t$ , the rank-one tensors of  $(\mathbf{a}_k \circ \mathbf{b}_k \circ \mathbf{c}_k)$  can be perceived as building blocks of the 3-dimensional egonet-tensors, and the “degree of presence” of community  $k$  at time  $t$  is captured by  $d_{tk}$ , while the constraint  $\|\tilde{\mathbf{d}}_t\|_1 = 1 \forall t$  resolves the scalar ambiguity by normalization. Indeed, stationary graphs with  $T = 1$  can be subsumed by this model, for which the additional constraints on  $\mathbf{D}$  reduce to the trivial solution for the fourth factor as  $\mathbf{D} = \mathbf{1}_{1 \times K}$ . Focusing on the  $n$ -th slab of  $\underline{\mathbf{W}}_t$ , the egonet adjacency of node  $n$  at time  $t$  is decomposed as

$$\mathbf{W}_t^{(n)} = \sum_{k=1}^K d_{tk} c_{nk} (\mathbf{a}_k \circ \mathbf{b}_k) \quad (17)$$

---

**Algorithm 4** Constrained ALS for time-varying graphs
 

---

Input  $\underline{\mathbf{W}}, K, I_{\max}, \lambda$   
 Initialize  $\mathbf{A}, \mathbf{B}, \mathbf{C} \in \mathbb{R}^{N \times K}$  and  $\mathbf{D} \in \mathbb{R}^{T \times K}$  and set  $k = 0$   
 Form matrix reshapes  $\mathbf{W}_1, \mathbf{W}_2, \mathbf{W}_3, \mathbf{W}_4$  of the tensor as  
 $\mathbf{W}_1 := [\text{vec}(\underline{\mathbf{W}}_{1,\dots,1}), \dots, \text{vec}(\underline{\mathbf{W}}_{1,\dots,N})]$   
 $\mathbf{W}_2 := [\text{vec}(\underline{\mathbf{W}}_{\cdot,1,\dots,1}), \dots, \text{vec}(\underline{\mathbf{W}}_{\cdot,1,\dots,N})]$   
 $\mathbf{W}_3 := [\text{vec}(\underline{\mathbf{W}}_{\cdot,\dots,1}), \dots, \text{vec}(\underline{\mathbf{W}}_{\cdot,\dots,N})]$   
 $\mathbf{W}_4 := [\text{vec}(\underline{\mathbf{W}}_{\cdot,\dots,1}), \dots, \text{vec}(\underline{\mathbf{W}}_{\cdot,\dots,T})]$   
**while**  $k < I_{\max}$  **do** or not-converged  
 $\mathbf{H}_A^{(k)} = \mathbf{D}^{(k-1)} \odot \mathbf{C}^{(k-1)} \odot \mathbf{B}^{(k-1)}$   
 $\mathbf{A}^{(k)} \leftarrow$  Algorithm 2 with input  $\{\mathbf{H}_A^{(k)}, \mathbf{W}_1, \mathbf{A}^{(k-1)}\}$   
 $\mathbf{H}_B^{(k)} = \mathbf{D}^{(k-1)} \odot \mathbf{C}^{(k-1)} \odot \mathbf{A}^{(k)}$   
 $\mathbf{B}^{(k)} \leftarrow$  Algorithm 2 with input  $\{\mathbf{H}_B^{(k)}, \mathbf{W}_2, \mathbf{B}^{(k-1)}\}$   
 $\mathbf{H}_C^{(k)} = \mathbf{D}^{(k-1)} \odot \mathbf{B}^{(k)} \odot \mathbf{A}^{(k)}$   
 $\mathbf{C}^{(k)} \leftarrow$  Algorithm 3 with input  $\{\mathbf{H}_C^{(k)}, \mathbf{W}_3, \mathbf{C}^{(k-1)}\}$   
 $\mathbf{H}_D^{(k)} = \mathbf{C}^{(k)} \odot \mathbf{B}^{(k)} \odot \mathbf{A}^{(k)}$   
 $\mathbf{D}^{(k)} \leftarrow$  Algorithm 3 with input  $\{\mathbf{H}_D^{(k)}, \mathbf{W}_4, \mathbf{D}^{(k-1)}\}$   
 $k \leftarrow k + 1$   
**end while**  
**Return**  $\mathbf{A}^{(k)}, \mathbf{B}^{(k)}, \mathbf{C}^{(k)}, \mathbf{D}^{(k)}$

---

where the product  $d_{tk}c_{nk}$  provides the association of node  $n$  to community  $k$  at time  $t$ .

Similar to (3), the decomposition in (15) is solved by alternating least-squares for updating the factors. The overall solver is provided in Alg. 4, within which we have utilized Alg. 2 and Alg. 3 for handling the emerging subproblems.

## VI. SIMULATED TESTS

In this section, the performance of the proposed EgoTen community detection algorithm is assessed via benchmark synthetic networks, as well as real-world datasets. Experiments over Lancicchinetti-Fortunatoand-Radicci (LFR) synthetic benchmarks enables us to simulate networks with different levels of community mixing, as well as number of overlapping nodes. This proves helpful in highlighting the enhanced capacity of community detection achieved by exploiting the ‘‘higher-order’’ properties of vertices captured in the proposed egonet-tensor.

### A. Benchmark networks

LFR benchmark networks provide synthetic graphs with ground-truth communities, in which certain properties of real-world networks, namely power-law distribution for nodal degrees as well as community sizes are preserved. LFR networks are configured to have a total number of  $N$  nodes (vertices), nodal average degree  $\bar{d}$ , exponent of degree distribution  $\gamma_1$ , and exponent of community-size distribution  $\gamma_2$ . Furthermore, *mixing parameter*  $\mu$  controls the community cohesion, where larger  $\mu$  induces more connections among nodes in different communities, thus generating less cohesive communities. Moreover, parameters  $\{o_n, o_m\}$  set the number of overlapping nodes, that is, nodes belonging to more than one community, and the number of communities with which these nodes are associated, respectively. We have compared the performance

of the proposed EgoTen with (similarly-constrained) nonnegative matrix factorization (NMF) schemes over the adjacency matrix, as well as other state-of-the-art community detection schemes.

1) *Matrix versus tensor factorization*: The experiments here focus on comparison between EgoTen and its matrix counterpart. In particular, we will demonstrate how the higher-order connectivity patterns as well as structured redundancy offered through EgoTen can increase the robustness of community detection in the case of overlapping, and highly-mixed communities.

To this end, the corresponding NMF approach aims at factorizing matrix  $\mathbf{W}$  by solving

$$\begin{aligned}
 & \min_{\mathbf{U}, \mathbf{V}} \|\mathbf{W} - \mathbf{U}\mathbf{V}^\top\|_F^2 \\
 & \text{s.t.} \quad \|\mathbf{u}_n\|_1 = 1 \forall n = 1, \dots, N, \mathbf{U} \geq \mathbf{0}, \mathbf{V} \geq \mathbf{0}
 \end{aligned} \tag{18}$$

where  $\mathbf{U}, \mathbf{V} \in \mathbb{R}^{N \times K}$ , and  $\mathbf{U}^\top := [\mathbf{u}_1, \mathbf{u}_2, \dots, \mathbf{u}_N]$ . Thus, similar to the nonnegative tensor decomposition in (3), the  $n$ -th row of matrix  $\mathbf{U}$  contains community association coefficients of node  $n$ , and is subject to a simplex constraint. This minimization is solved via the AO-ADMM toolbox in [43]. Hard community assignments resulting from the factor  $\mathbf{U}$  can be achieved similar to the procedure over the  $\hat{\mathbf{C}}$  factor in EgoTen, as discussed in Section IV.

In our experiments, we have generated LFR networks with  $N = 1,000$ ,  $\gamma_1 = 2$ ,  $\gamma_2 = 1$ , average degree  $\bar{d} = 100$ , and  $o_m = \{2, 3, 5\}$ . To demonstrate the robustness of EgoTen, Fig. 5 shows the performance of EgoTen in comparison with constrained NMF over the adjacency matrix versus different values of  $\mu$ , in terms of the NMI, and the F1-score. The experiments have been carried out for  $o_n = 200$  (20%) number of overlapping nodes, upperbound on the number of communities is set as  $K = 3|\mathcal{C}|$ , and  $\tau$  is chosen so that the highest NMI is achieved for both methods. Furthermore, Fig. 6 depicts the performance of NMF and EgoTen across different levels of overlap, controlled through the number of overlapping nodes  $o_n$ , while fixing  $\mu = 0.2$ . In addition, since a common practical concern is the lack of knowledge over the number of communities, Fig. 7 studies the robustness of NMF and EgoTen to this factor, by setting  $K = m|\mathcal{C}|$ , and varying  $m \in [1.2, 5]$ . As the plots in Figures 5-7 corroborate, capturing the higher-order connectivity patterns of the vertices and the structured decomposition of reinforced egonet-tensor improve robustness of nonnegative factorization methods against community coherence, presence of overlapping nodes, as well as rough estimates of the number of communities.

2) *EgoTen vs. state-of-the-art methods*: In this subsection, we compare the performance of EgoTen with state-of-the-art competitors, namely Osloom [47], Bigclam [9], Infomap [48], and Louvain [5]. Similar to the previous subsection, we have generated LFR networks with  $N = 1,000$ ,  $\gamma_1 = 2$ ,  $\gamma_2 = 1$  and  $o_m = \{2, 3, 5\}$ . Number of overlapping nodes  $o_n$  as well as mixing parameter  $\mu$  are varied in the range [10, 600] and [0.1, 0.7], respectively. Threshold parameter for assigning hard

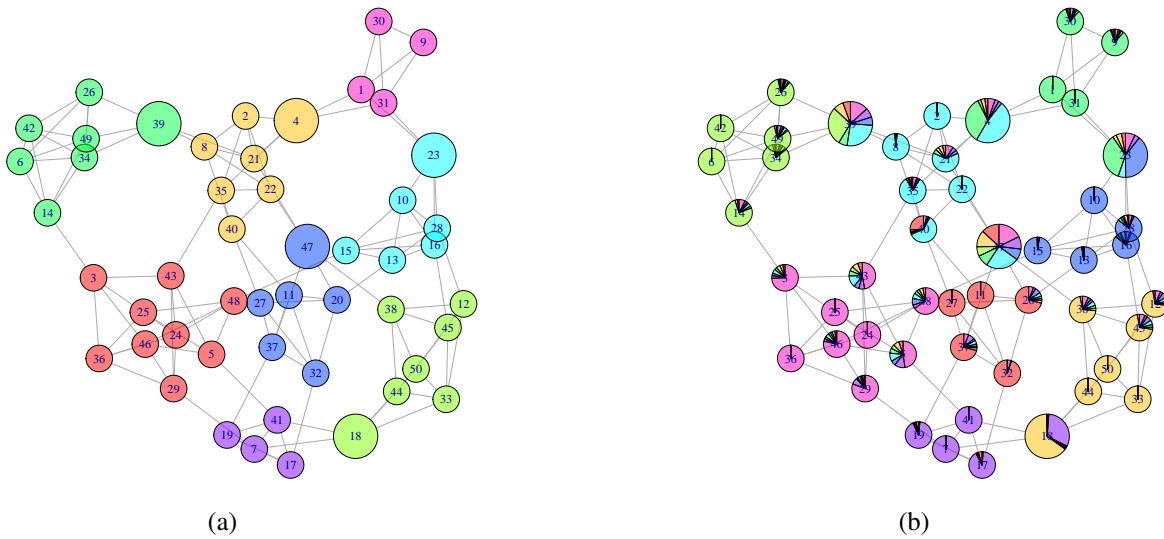


Fig. 4: Visualization of an LFR network with  $N = 50$ ,  $\mu = 0.2$ , and five “shared” nodes  $\{4, 18, 23, 39, 47\}$ , represented by a larger radius, with (a) hard community association via Infomap; and (b) soft association via EgoTen. Pie-charts depict association ratios.

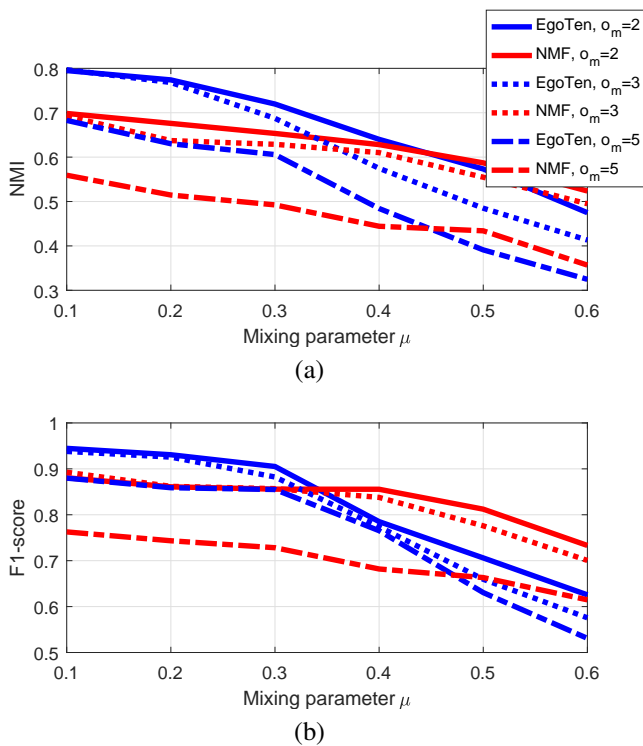


Fig. 5: Performance of constrained NMF and EgoTen in terms of (a) NMI; and, (b) average F1-score, versus  $\mu$  for LFR networks of  $N = 1,000$ , with  $o_n = 200$ .

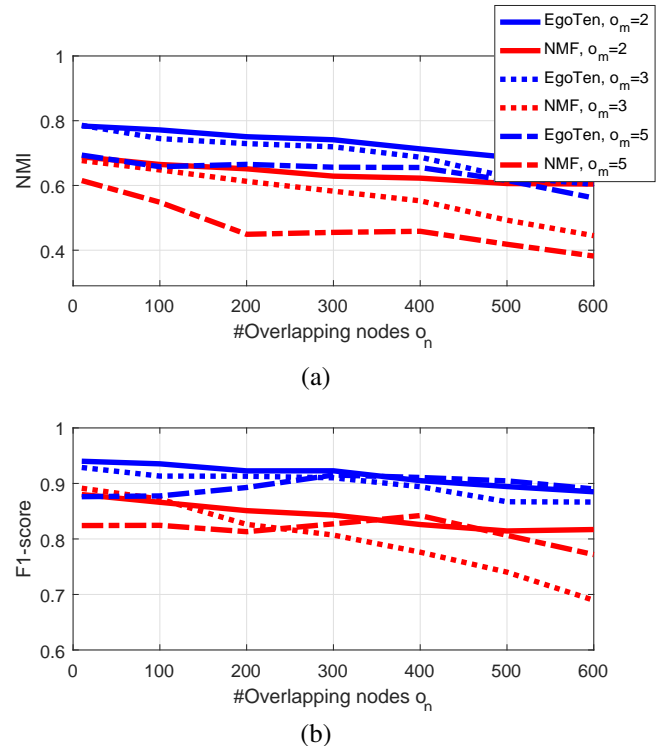


Fig. 6: Performance of constrained NMF and EgoTen in terms of (a) NMI; and, (b) average F1-score, versus  $o_n$  for LFR networks with  $N = 1,000$ , and  $\mu = 0.2$ .



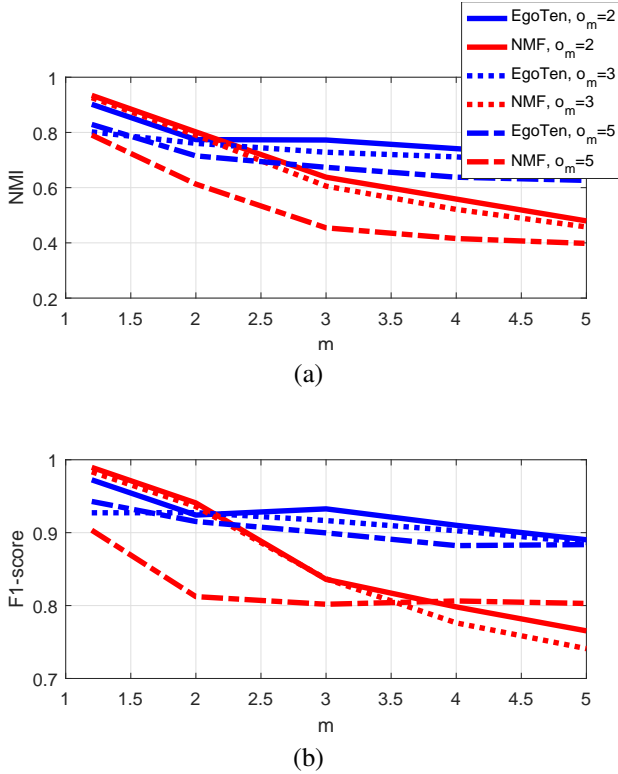


Fig. 7: Performance of constrained NMF and EgoTen in terms of (a) NMI; and, (b) average F1-score, versus upperbound on community number  $K = m|C|$  parametrized by  $m$  for LFR networks with  $N = 1,000$ ,  $o_n = 300$  and  $\mu = 0.2$ .

community memberships of EgoTen is chosen as<sup>1</sup>  $\tau = 1/K$ .

Performance is reported in terms of NMI, and F1-score. As Figures 8 and 9 corroborate, EgoTen offers the highest performance for a wide range of  $\mu$ , as well as  $o_n$ , thanks to the reinforced structure of the egonet-tensor.

Regarding the scalability of the proposed EgoTen algorithm, Fig. 10 depicts run time versus network size  $N$  while average nodal degree is kept constant at  $\bar{d} = 100$ . As the plot corroborates, exploitation of the sparsity in the egonet-tensor provides the algorithm with scalability, while the same can not be claimed for all other competitors.

### B. Time-varying graphs

In this subsection, the performance of the proposed EgoTen in Alg. 4 for community identification over time-varying networks is assessed. To this end, we have generated a synthetic network with  $N = 1,000$  nodes for a span of  $T = 20$  slots. Initially at  $t = 1$ , the networks is generated with two distinct communities, each containing of 500 nodes. For  $t > 1$ , the community association of 600 randomly selected nodes remains unchanged, whereas the other 400 nodes migrate from

<sup>1</sup>Since we have imposed a simplex constraint over the  $K$  association indices for any given node,  $\tau = 1/K$  could be interpreted as having an association index higher than an equal association with all detected communities. Other selection schemes for  $\tau$ , for instance setting to the value providing the community cover with the smallest average conductance, are also viable.

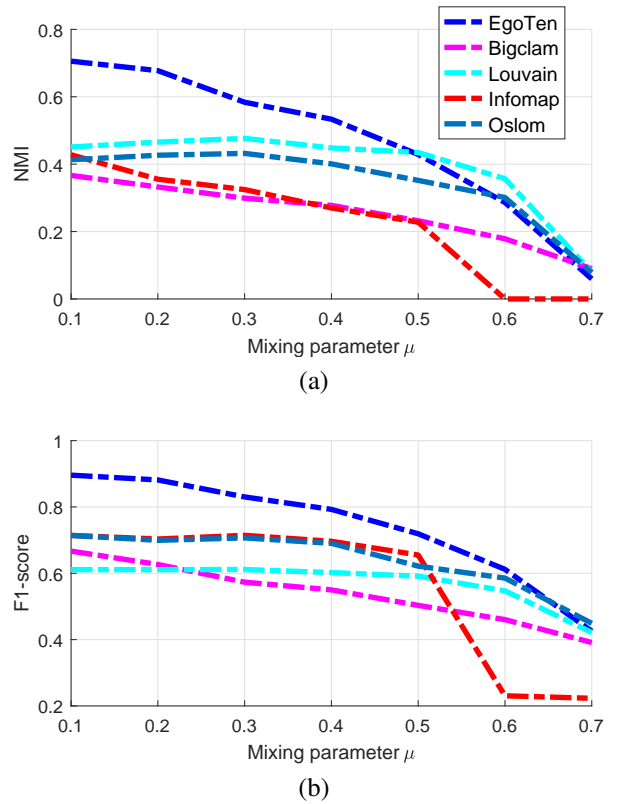


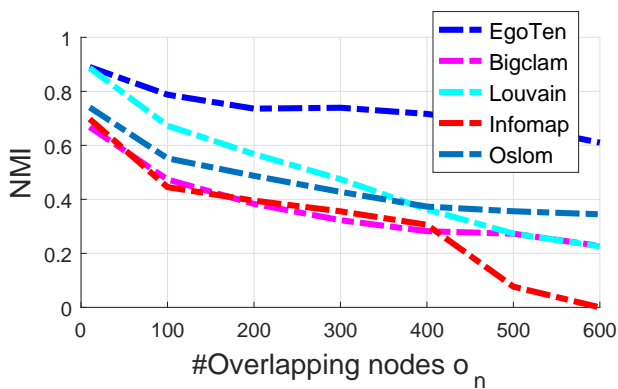
Fig. 8: Performance of EgoTen and state-of-the-art algorithms in terms of (a) NMI; and, (b) average F-1 score, for LFR networks of  $N = 1,000$ ,  $o_n = 300$ , and  $o_m = 5$  versus  $\mu$ .

their original community to a third newly-formed community. Transition slot  $\tau_n$  for each of these nodes is identically drawn from a normal distribution  $\mathcal{N}(10, 1)$ . For any time slot  $t$ , the network edges are drawn according to a block stochastic model, where nodes within the same community are connected with probability 0.3, and out-of-community edges are drawn with probability 0.1. EgoTen's performance is compared with that of constrained NMF, for which  $\mathbf{U}$  and  $\mathbf{V}$  per  $t$  is used as initialization for  $t+1$  to provide NMF with consistency across time.

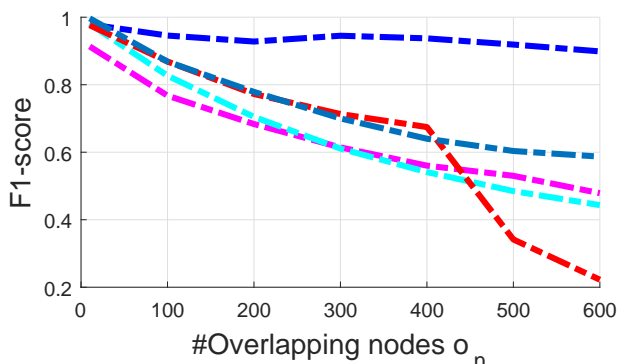
Performance is measured in terms of NMI, and it is averaged over 20 realizations of the network in Fig. 12. Furthermore, Fig. 13 illustrates the identified communities for different nodes across time for a realization. That is, for any  $t$  on the x-axis, nodes associated with the same community are shown with the same color. The plot depicts ground truth as well as EgoTen and NMF results, where we have perturbed ordering of nodes for a better visualization. Clearly, EgoTen successfully identifies the two initial communities, as well as three communities after the migration of a subset of nodes, presenting solid blocks similar to those in the ground truth, while communities detected via constrained NMF are of lower quality.

### C. Real world Networks

In this section EgoTen is utilized for performing community detection on a number of real-world networks, tabulated in



(a)



(b)

Fig. 9: Performance of EgoTen and state-of-the-art algorithms in terms of (a) NMI; and, (b) average F1-score, for LFR networks of  $N = 1,000$ ,  $\mu = 0.2$ , and  $o_m = 5$  versus  $o_n$ .

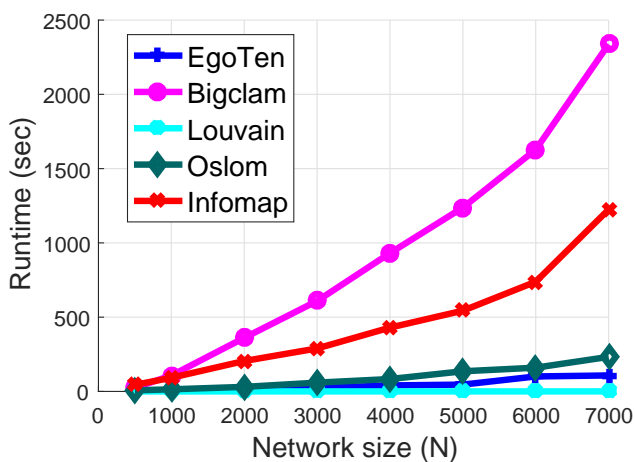


Fig. 10: Scalability of different algorithms as  $N$  grows.

Table I. To study the quality of detected communities for real-world networks -whose ground truth community association is often unavailable- we examine the conductance of detected communities. In particular, given a cover  $\mathcal{C} = \{\mathcal{C}_1, \dots, \mathcal{C}_K\}$ , let us compute the conductance  $\phi(\mathcal{C}_i)$  for  $i = 1, \dots, K$ . Corresponding to a value  $\nu \in [0, 1]$ , let us define the set of communities whose conductance is less than  $\nu$ , i.e.,

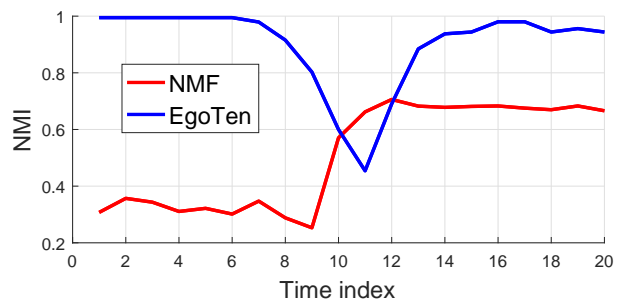


Fig. 11: NMI for the detected communities across time for synthetic time-varying graphs.

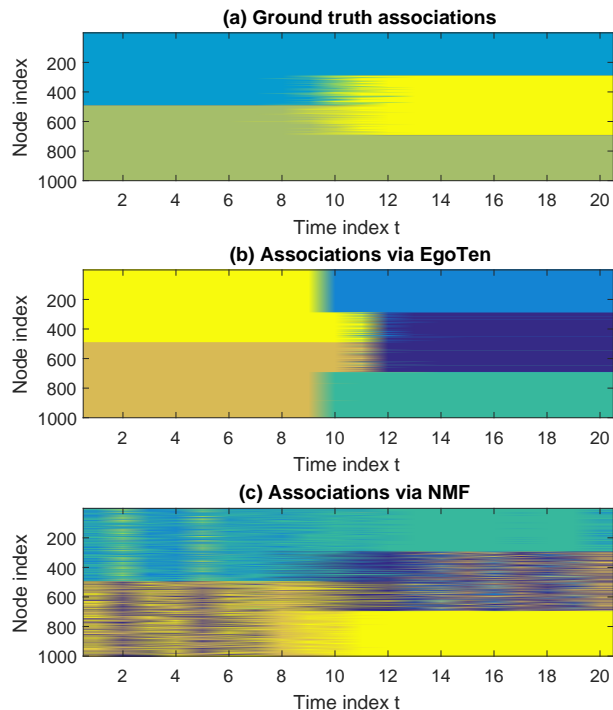


Fig. 12: Time-varying community association of nodes, where same communities are color-coded similarly; thus, for a given  $t$  on the x-axis, nodes in a community have the same color in (a) ground truth; and results via (b) EgoTen; and, (c) NMF.

$\mathcal{S}_\nu := \{\mathcal{C}_j | \phi(\mathcal{C}_j) < \nu\}$ . Then, coverage( $\nu$ ) is defined as

$$\text{coverage}(\nu) := \frac{\left| \bigcup_{\mathcal{C}_i \in \mathcal{S}_\nu} \mathcal{C}_i \right|}{N} \quad (19)$$

Consequently, conductance-coverage curve is plotted by varying the value  $\nu$  from 0 to 1 on the  $y$ -axis and reporting the corresponding coverage value on the  $x$ -axis. As low values of conductance correspond to more cohesive communities, smaller area under curve (AUC) implies better performance. Fig. 12 plots the coverage-conductance curve and Table II tabulates AUC as well as average conductance defined in (14). Since Louvain does not allow for overlapping nodes, the two metrics coincide, hence the corresponding one column in Tabel

II. As the results corroborate, the quality of detected communities via EgoTen is closely competing or outperforming the ones provided by other methods, while it remains robust to “resolution limit” [49] observed in Osloom in Fig. 12 (a) and Infomap in Fig. 12 (d) whose performance are limited to detecting only large communities.

TABLE I: Real-world networks.

$r_a$	Size $N$	Edges
Dolphins	62	159
Les miserable	77	254
Football	115	613
Facebook	4039	88,234

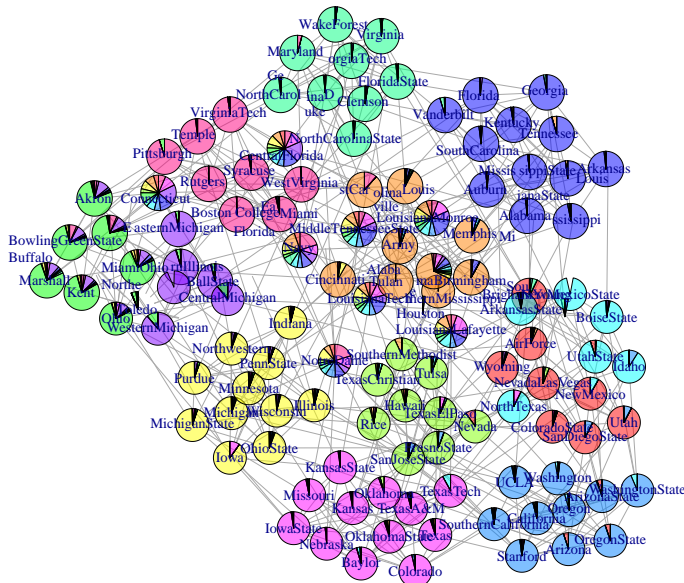


Fig. 13: Visualization of the American College Football Network with  $N = 115$  and  $K = 12$ . Different colors correspond to different detected communities, and the pie-charts reveal soft community association of the nodes.

## VII. CONCLUSION AND REMARKS

By viewing networks as the union of nodal egonets, a novel tensor-based representation for capturing high-order nodal connectivities has been introduced. The induced redundancy in the constructed egonet-tensor bestows the novel representation with rich structure, and is utilized for community detection by casting the problem as a constrained tensor decomposition task. Utilization of tensor sparsity as well as parallel computation endow the algorithm with scalability, while the structured redundancy enhances the performance against overlapping and highly-mixed communities. The proposed framework is broadened to accommodate time-varying graphs, where a four-dimensional tensor enables simultaneous community identification over the entire horizon yielding an improved performance.

As a natural extension, one can generalize the tensor-based representation to account for adjacency matrices capturing

the connectivity of  $2, 3, \dots, d_{\max}$ -hop neighbors. This approach indeed highlights the tradeoff between flexibility and redundancy, as memory and computational intensity of the corresponding CPD as well as proper tuning of parameters will influence the quality of the detected communities. One could analyze this tradeoff to further characterize how the quality of detected communities evolves as the coverage of *extended-egonets* increases; however, this goes beyond the scope of this work, and is left for future investigation.

## REFERENCES

- [1] J. D. Power, A. L. Cohen, S. M. Nelson, G. S. Wig, K. A. Barnes, J. A. Church, A. C. Vogel, T. O. Laumann, F. M. Miezin, B. L. Schlaggar, and S. E. Petersen, “Functional network organization of the human brain,” *Neuron*, vol. 72, no. 4, pp. 665–678, Nov. 2011.
- [2] Y. R. Lin, Y. Chi, S. Zhu, H. Sundaram, and B. L. Tseng, “Analyzing communities and their evolutions in dynamic social networks,” *ACM Trans. on Knowledge Discovery from Data*, vol. 3, no. 2, p. 8, April 2009.
- [3] S. Papadopoulos, Y. Kompatsiaris, A. Vakali, and P. Spyridonos, “Community detection in social media,” *Data Mining and Knowledge Discovery*, vol. 24, no. 3, pp. 515–554, 2012.
- [4] P. K. Reddy, M. Kitsuregawa, P. Sreekanth, and S. S. Rao, “A graph-based approach to extract a neighborhood customer community for collaborative filtering,” *Intl. Workshop on Databases in Networked Information Systems*, pp. 188–200, 2002.
- [5] V. D. Blondel, J.-L. Guillaume, R. Lambiotte, and E. Lefebvre, “Fast unfolding of communities in large networks,” *Journal of Statistical Mechanics: Theory and Experiment*, vol. 2008, no. 10, pp. P10008:1–12, 2008.
- [6] J. Duch and A. Arenas, “Community detection in complex networks using extremal optimization,” *Physical Review E*, vol. 72, no. 2, pp. 027104:1–4, 2005.
- [7] E. M. Airolidi, D. M. Blei, S. E. Fienberg, and E. P. Xing, “Mixed membership stochastic blockmodels,” *Advances in Neural Information Processing Systems*, pp. 33–40, Vancouver, Canada, Dec. 2009.
- [8] A. Anandkumar, R. Ge, D. Hsu, and S. M. Kakade, “A tensor approach to learning mixed membership community models,” *Journal of Machine Learning Research*, vol. 15, no. 1, pp. 2239–2312, Jan. 2014.
- [9] J. Yang and J. Leskovec, “Overlapping community detection at scale: a nonnegative matrix factorization approach,” *Proc. of ACM Intl. Conf. on Web Search and Data Mining*, pp. 587–596, Rome, Italy, Feb. 2013.
- [10] I. Derényi, G. Palla, and T. Vicsek, “Clique percolation in random networks,” *Physical Review Letters*, vol. 94, no. 16, pp. 160202–1:4, April 2005.
- [11] U. Von Luxburg, “A tutorial on spectral clustering,” *Statistics and Computing*, vol. 17, no. 4, pp. 395–416, Aug. 2007.
- [12] F. Wang, T. Li, X. Wang, S. Zhu, and C. Ding, “Community discovery using nonnegative matrix factorization,” *ACM Trans. on Data Mining and Knowledge Discovery*, vol. 22, no. 3, pp. 493–521, July 2011.
- [13] X. Cao, X. Wang, D. Jin, Y. Cao, and D. He, “Identifying overlapping communities as well as hubs and outliers via nonnegative matrix factorization,” *Scientific Reports*, vol. 3, p. 2993, 2013.
- [14] I. Psorakis, S. Roberts, M. Ebdon, and B. Sheldon, “Overlapping community detection using Bayesian non-negative matrix factorization,” *Physical Review E*, vol. 83, no. 6, p. 066114, 2011.
- [15] Y. Zhang and D.-Y. Yeung, “Overlapping community detection via bounded nonnegative matrix tri-factorization,” *Proc. of ACM Intl. Conf. on Knowledge Discovery and Data Mining*, pp. 606–614, 2012.
- [16] Z.-Y. Zhang, Y. Wang, and Y.-Y. Ahn, “Overlapping community detection in complex networks using symmetric binary matrix factorization,” *Physical Review E*, vol. 87, no. 6, p. 062803, 2013.
- [17] S. Fortunato, “Community detection in graphs,” *Physics Reports*, vol. 486, no. 3, pp. 75–174, Feb. 2010.
- [18] S. Fortunato and D. Hric, “Community detection in networks: A user guide,” *Physics Reports*, vol. 659, pp. 1–44, 2016.
- [19] J. J. Whang, D. F. Gleich, and I. S. Dhillon, “Overlapping community detection using seed set expansion,” *Proc. of ACM Intl. Conf. on Information and Knowledge Management*, pp. 2099–2108, 2013.
- [20] K. He, Y. Sun, D. Bindel, J. Hoyer, and Y. Li, “Detecting overlapping communities from local spectral subspaces,” *IEEE Intl. Conf. on Data Mining*, pp. 769–774, 2015.

TABLE II: Quality of detected cover on real-world networks in terms of AUC and average conductance.

	EgoTen			Bigclam			Louvain		Infomap			Oslo		
	$ \mathcal{C} $	AUC	$\bar{\phi}(\mathcal{C})$	$ \mathcal{C} $	AUC	$\bar{\phi}(\mathcal{C})$	$ \mathcal{C} $	AUC (or $\bar{\phi}(\mathcal{C})$ )	$ \mathcal{C} $	AUC	$\bar{\phi}(\mathcal{C})$	$ \mathcal{C} $	AUC	$\bar{\phi}(\mathcal{C})$
Dolphins	10	0.2984	0.4584	5	0.6176	0.6176	11	0.3902	10	0.3201	0.4012	2	0.1034	0.1034
Les miserable	5	0.2803	0.2803	10	0.6042	0.4666	15	0.3343	12	0.3534	0.4052	3	0.2127	0.2182
Football	15	0.4085	0.3480	15	0.4989	0.4101	15	0.3752	12	0.3974	0.3468	11	0.3430	0.3037
Facebook	100	0.3768	0.4931	100	0.3798	0.4973	100	0.1329	5	0.0370	0.0360	110	0.4998	0.4955

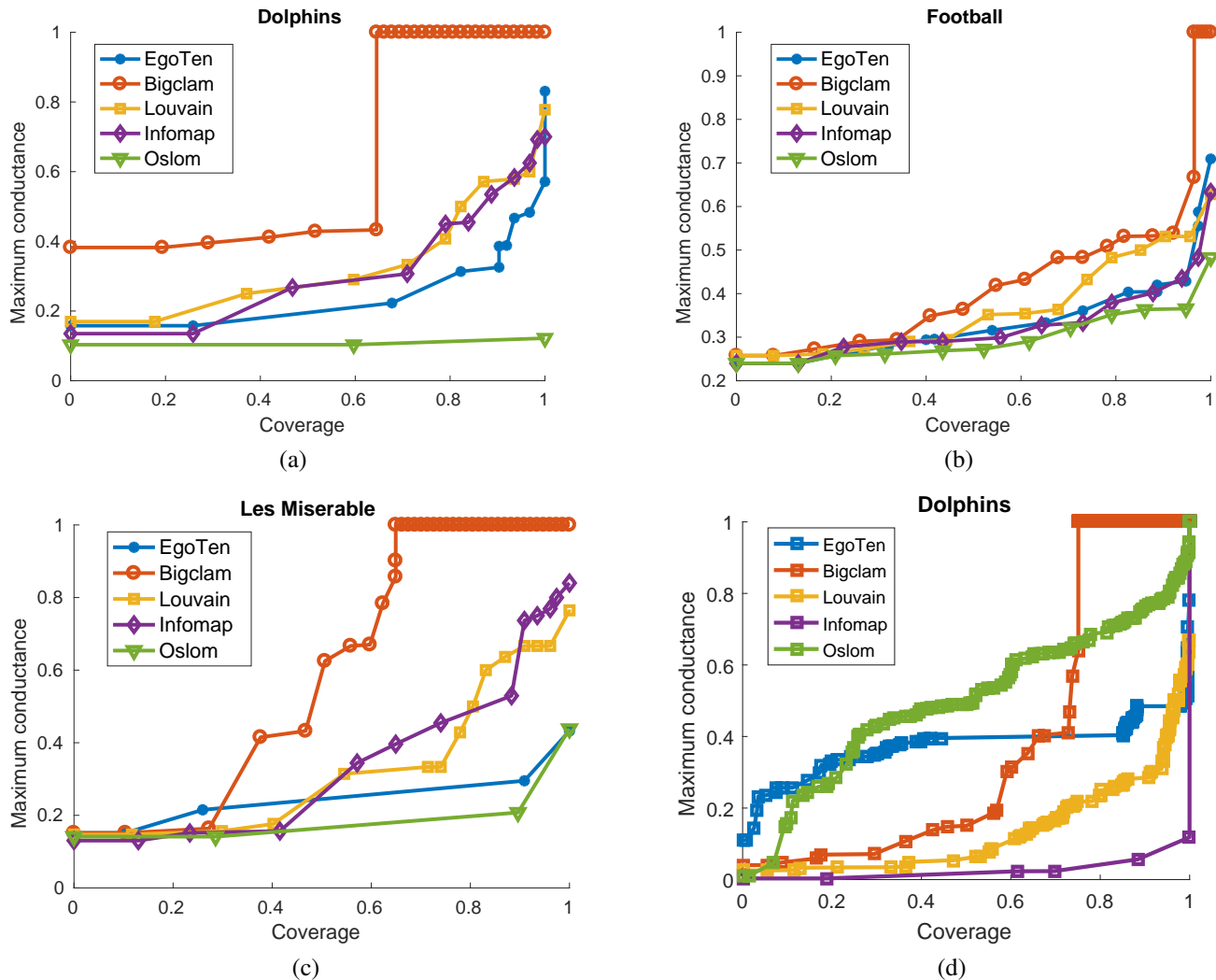


Fig. 14: Maximum-conductance versus coverage for real-world networks with underlying community structure. Lower curves correspond to better performance.

- [21] J. J. Whang, I. S. Dhillon, and D. F. Gleich, "Non-exhaustive, overlapping k-means," *Proc. of SIAM Intl. Conf. on Data Mining*, pp. 936–944, 2015.
- [22] E. E. Papalexakis, L. Akoglu, and D. Ience, "Do more views of a graph help? Community detection and clustering in multi-graphs," *IEEE Intl. Conf. on Information Fusion*, pp. 899–905, 2013.
- [23] E. E. Papalexakis, N. D. Sidiropoulos, and R. Bro, "From k-means to higher-way co-clustering: Multilinear decomposition with sparse latent factors," *IEEE Trans. on Signal Processing*, vol. 61, no. 2, pp. 493–506, Jan. 2013.
- [24] J. Yang, J. McAuley, and J. Leskovec, "Community detection in networks with node attributes," *IEEE Intl. Conf. on Data Mining*, pp. 1151–1156, 2013.
- [25] M. Araujo, S. Papadimitriou, S. Günnemann, C. Faloutsos, P. Basu, A. Swami, E. E. Papalexakis, and D. Koutra, "Com2: Fast automatic discovery of temporal (comet) communities," *Pacific-Asia Conf. on Knowledge Discovery and Data Mining*, pp. 271–283, 2014.
- [26] B. Baingana and G. B. Giannakis, "Joint community and anomaly tracking in dynamic networks," *IEEE Transactions on Signal Processing*, vol. 64, no. 8, pp. 2013–2025, 2016.
- [27] F. Huang, U. Niranjan, M. U. Hakeem, and A. Anandkumar, "Online tensor methods for learning latent variable models," *Journal of Machine Learning Research*, vol. 16, pp. 2797–2835, 2015.
- [28] F. Sheikholeslami, B. Baingana, G. B. Giannakis, and N. D. Sidiropoulos, "Egonet tensor decomposition for community identification," *Proc. of Globalsip*, Washington, DC, Dec. 2016.
- [29] A. R. Benson, D. F. Gleich, and J. Leskovec, "Tensor spectral clustering for partitioning higher-order network structures," *Proc. of SIAM Intl. Conf. on Data Mining*, pp. 118–126, Vancouver, Canada, Feb. 2015.
- [30] T. G. Kolda, B. W. Bader, and J. P. Kenny, "Higher-order web link analysis using multilinear algebra," *IEEE Intl. Conf. on Data Mining*, pp. 8–pp, 2005.
- [31] J. Kruskal, "Three-way arrays: Rank and uniqueness of trilinear decompositions, with application to arithmetic complexity and statistics,"

- Linear Algebra and its Applications*, vol. 18, no. 2, pp. 95–138, 1977.
- [32] N. Sidiropoulos and R. Bro, “On the uniqueness of multilinear decomposition of N-way arrays,” *Journal of Chemometrics*, vol. 14, no. 3, pp. 229–239, June 2000.
- [33] L. Chiantini and G. Ottaviani, “On generic identifiability of 3-tensors of small rank,” *SIAM J. Matrix Analysis Applications*, vol. 33, no. 3, pp. 1018–1037, 2012.
- [34] L. Akoglu, M. McGlohon, and C. Faloutsos, “Oddball: Spotting anomalies in weighted graphs,” *Advances in Knowledge Discovery and Data Mining*, pp. 410–421, 2010.
- [35] J. Leskovec and J. J. McAuley, “Learning to discover social circles in ego networks,” *Advances in Neural Information Processing Systems*, pp. 539–547, 2012.
- [36] C. Lan, Y. Yang, X. Li, B. Luo, and J. Huan, “Learning social circles in ego networks based on multi-view social graphs,” *arXiv preprint arXiv:1607.04747*, 2016.
- [37] T. G. Kolda and B. W. Bader, “Tensor decompositions and applications,” *SIAM review*, vol. 51, no. 3, pp. 455–500, 2009.
- [38] E. E. Papalexakis, C. Faloutsos, and N. D. Sidiropoulos, “Parcube: Sparse parallelizable tensor decompositions,” *Joint European Conf. on Machine Learning and Knowledge Discovery in Databases*, pp. 521–536, Bristol, UK, 2012.
- [39] S. Smith and G. Karypis, “SPLATT: The Surprisingly Parallel sparse Tensor Toolkit,” <http://cs.umn.edu/~splatt/>.
- [40] M. Mardani, G. Mateos, and G. B. Giannakis, “Subspace learning and imputation for streaming big data matrices and tensors,” *IEEE Trans. on Signal Processing*, vol. 63, no. 10, pp. 2663 – 2677, May 2015.
- [41] J. A. Bazerque, G. Mateos, and G. B. Giannakis, “Rank regularization and bayesian inference for tensor completion and extrapolation,” *IEEE Trans. on Signal Processing*, vol. 61, no. 22, pp. 5689–5703, Nov. 2013.
- [42] G. B. Giannakis, Q. Ling, G. Mateos, I. D. Schizas, and H. Zhu, “Decentralized learning for wireless communications and networking,” *Splitting Methods in Communication, Imaging, Science, and Engineering*, pp. 461–497, Springer, 2016.
- [43] K. Huang, N. D. Sidiropoulos, and A. P. Liavas, “A flexible and efficient algorithmic framework for constrained matrix and tensor factorization,” *arXiv preprint arXiv:1506.04209*, 2015.
- [44] J. Duchi, S. Shalev-Shwartz, Y. Singer, and T. Chandra, “Efficient projections onto the  $l_1$ -ball for learning in high dimensions,” *Proc. Intl. Conf. on Machine Learning*, pp. 272–279, 2008.
- [45] A. Lancichinetti, S. Fortunato, and J. Kertész, “Detecting the overlapping and hierarchical community structure in complex networks,” *New Journal of Physics*, vol. 11, no. 3, p. 033015, 2009.
- [46] J. Leskovec, K. J. Lang, A. Dasgupta, and M. W. Mahoney, “Community structure in large networks: Natural cluster sizes and the absence of large well-defined clusters,” *Internet Mathematics*, vol. 6, no. 1, pp. 29–123, 2009.
- [47] A. Lancichinetti, F. Radicchi, J. J. Ramasco, and S. Fortunato, “Finding statistically significant communities in networks,” *PLoS one*, vol. 6, no. 4, p. e18961, 2011.
- [48] L. Bohlin, D. Edler, A. Lancichinetti, and M. Rosvall, “Community detection and visualization of networks with the map equation framework,” *Measuring Scholarly Impact*, pp. 3–34, 2014.
- [49] S. Fortunato and M. Barthelemy, “Resolution limit in community detection,” *Proc. of the National Academy of Sciences*, vol. 104, no. 1, pp. 36–41, 2007.